




A phenomenological constitutive model for the viscoelastic deformation of elastomers

Vinotharan Annarasa¹ · Atanas A. Popov¹ ·
Davide S.A. De Focatiis¹ 

Received: 5 April 2019 / Accepted: 6 May 2020 / Published online: 21 May 2020
© The Author(s) 2020

Abstract This study proposes a one-dimensional constitutive model for elastomeric materials based on recent observations regarding the separation of elastic and viscous contributions in uniaxial cyclic tensile experiments on EPDM rubber. The focus is on capturing the changes in constitutive behavior and energy dissipation associated with the Mullins effect. In the model, this is achieved through the evolution of both permanent set and hyperelastic parameters of an Edwards-Vilgis function to account for the Mullins effect, and with a viscosity associated with the effective stretch rate of the network to describe the non-linear flow stress. The simulations are able to reproduce the observed constitutive response and its change with increasing levels of pre-deformation. The model is less able to accurately reproduce the virgin loading response, which is achieved via extrapolation to zero pre-strain. However, for practical purposes, where scragging of elastomeric products is the norm, the model is able to predict the cyclic response and the dissipated energy, and their change with different scragging levels in good agreement with experimental data.

Keywords Constitutive model · Mullins effect · EPDM rubber

1 Introduction

Elastomers are essential to a wide range of industrial applications, including tyres, dampers and seals to name a few. Constitutive models are a critical element in the design process to enable simulation of the in-service behavior of these products during their life cycle. Owing to stress softening, permanent set and viscoelasticity, amongst others, these materials exhibit a complex mechanical response. Furthermore, there is still much debate in the academic literature regarding the physical origins of several aspects of the underlying material behavior. A combination of the two factors described above has resulted in numerous modeling approaches being suggested by the research community.

✉ D.S.A. De Focatiis
davide.defocatiis@nottingham.ac.uk

¹ University of Nottingham, Nottingham NG7 2RD, UK

A significant stress softening is noted for rubber-like materials after an initial loading. This phenomenon is referred to as the Mullins effect (Mullins 1948; Mullins and Tobin 1965, 1957), and remains a major hurdle in the formulation of constitutive models, with the majority of rubber models still limited to behavior following a single prescribed preconditioning history. Several authors have attributed this phenomenon to bond rupture (Clough et al. 2016), molecular slippage (Houwink 1956), filler rupture (Kraus et al. 1966), molecular disentanglement (Hanson et al. 2005) and multiple networks (Fukahori 2005), although the cause of this phenomenon is still the subject of on-going research. Nevertheless, there are a limited number of physically motivated and phenomenological constitutive models that address the Mullins effect.

Marckmann et al. (2002) implemented a network alteration model, which considers the rupture of filler-matrix and polymer chain bonds (i.e. weak interactions and cross-links). As the bonds break, the average number of monomer segments N in a polymer chain increases. The parameter N is described by a linear function of the maximum pre-deformation seen by the network and is determined empirically. As N increases, the average number of active chains per unit volume n decreases, causing a softening of the network.

Mullins and Tobin (1957) suggested a two-phase model; the soft phase is the rubber matrix and the hard phase is the filler. The hard phase is initially surrounded by bound rubber from the soft phase, immobilized by means of entanglements and intermolecular forces. The softening effect arises from the release of bound rubber into the soft phase as a result of deformation and causes an increase in the effective volume of the soft phase. Models of this type were later implemented by Qi and Boyce (2004), and by Fernandes (2016). The former fits the initial and final volume fractions via optimization with respect to experimental data, whereas in the latter the effective volume of the soft phase was obtained by thermogravimetric analysis and swelling experiments.

Phenomenological descriptions of the Mullins phenomenon are broadly based on a concept introduced by Simo (1987), where strain energy density functions used to describe hyperelastic materials are multiplied by a reducing parameter. These models differ from each other in their definition of the damage variable, and they have been comprehensively reviewed by Diani et al. (2009).

Alongside stress softening, deformed elastomers exhibit a residual strain (or permanent set) on load removal. Simo's theory (Simo 1987) can be extended to account for permanent set by incorporating additional reducing parameters. An approach of this type has been followed by Dorfmann and Ogden (2004), and by Peña (2014). Maher et al. (2012) suggested an alternative approach, where an additive split of the stress tensor is used to capture the permanent set such that a negative stress is observed at a strain of zero; this is analogous to having a residual strain at a zero stress.

This paper presents a newly developed constitutive model whose parameter evolution leads to a Mullins effect and permanent set. This model is inspired by a recent study by De Focatiis et al. (2009) involving cyclic tests following various levels of pre-deformation where the elastic and viscous contributions were extracted from the stress-stretch response. By isolating the elastic response, they demonstrated that the parameters of an Edwards-Vilgis (E-V) strain energy function (Edwards and Vilgis 1986) fitted to the elastic contribution evolve with pre-deformation. Once permanent set was accounted for, the viscosity obtained from the isolated viscous contribution was shown to be independent of pre-deformation and a unique function of network stretch. Although non-linear viscosities have been incorporated in previous constitutive models, to the best of the authors' knowledge, none have been linked to strain in elastomers.

This paper formulates a one-dimensional (1D) constitutive model based on the ideas of an evolving hyperelastic component and a non-linear viscoelastic Maxwell element. It then

explores the extent to which such a model can capture the observed cyclic response and the dissipated energy of an EPDM rubber deformed in a series of complex strain histories. Although the implementation is currently only one-dimensional, the process of extending the model to 3D is discussed.

2 Materials and methods

The experimental data employed in this study have been described previously (De Focatiis et al. 2009), and only a brief overview of the experimental procedure is given here.

2.1 Materials and manufacturing

A carbon-black filled (50 phr) EPDM rubber was compression molded for 13 minutes at 160 °C into approximately 0.5 mm thick sheets. Uniaxial tensile test specimens were cut from the sheet using a hand operated Wallace specimen cutting press fitted with a dumbbell shaped cutter 1BA according to BS ISO 527-2.

2.2 Mechanical testing

Uniaxial tensile cyclic tests were performed on an Instron 4204 tensile testing machine fitted with a counterbalanced traveling extensometer to record the strain at a constant nominal strain rate of 0.03 s^{-1} at room temperature, $(24 \pm 1)^\circ\text{C}$. The specimens were subjected to four load-unload cycles through to a specified pre-deformation λ_{\max} , as illustrated in the inset of Fig. 1, and ten separate λ_{\max} increments between 1 and 6 inclusive were explored. To prevent buckling, the specimens were always unloaded to a stretch $\lambda_{(0.1\text{N})}$ corresponding to a small tensile force of 0.1 N.

Representative stress-stretch responses to the cyclic loading are illustrated in Fig. 1. Many of the characteristic features of the deformation of filled elastomers can be observed, including stress softening, permanent set and hysteresis. The stress softening and permanent set increase with increasing stretch λ .

3 Experimental analysis

3.1 Extraction of the elastic and viscous contributions

Decompositions into elastic and viscous contributions are commonly used in constitutive models describing elastomers and polymers, as first suggested by Haward and Thackray (1968), and as implemented by Bergström and Boyce (1998), and several others. In this study, it is assumed that the changes to the constitutive behavior of the rubber due to the Mullins effect arise as a result of the maximum level of deformation experienced, and hence simply depend on λ_{\max} . As subsequent unloading-reloading loops are similar (see Fig. 1), any unloading-reloading loops following λ_{\max} can be used in the decoupling of the mechanical response. The third unload-reload loop has been chosen in this instance since the constitutive response shows the most dramatic change in the first few cycles.

The assumption is that the steady-state response at a given strain level can be decomposed as the sum of an elastic (equilibrium) σ_e and a dissipative, or viscous σ_v stress. σ_v changes sign depending on the sign of the strain rate, positive on loading and negative on unloading.

Fig. 1 The stress-stretch response of selected EPDM specimens subjected to cyclic loading as shown in the inset to maximum stretches λ_{\max} of 2, 3, 4, 5 and 6. The specimens are unloaded to a stretch corresponding to a load of 0.1 N ($\lambda_{(0.1N)}$) to prevent buckling. A virgin specimen was used for each test

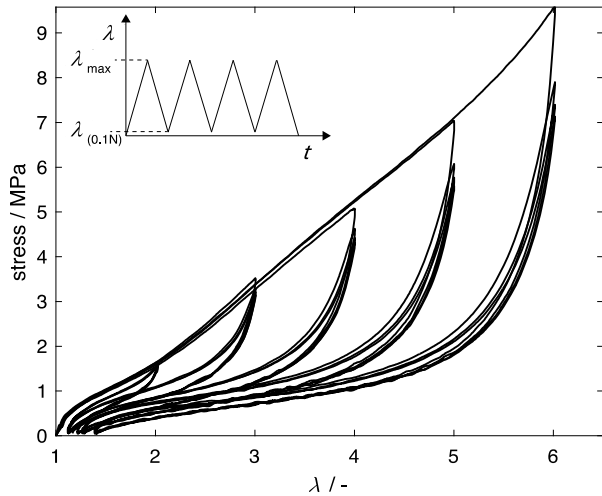
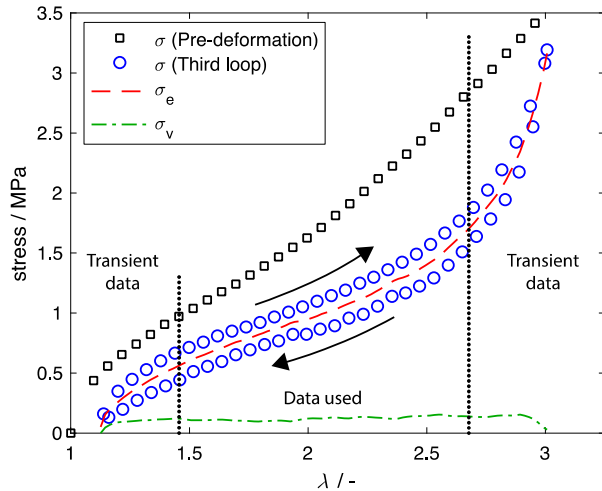


Fig. 2 The experimental stress-stretch response (symbols) to cyclic tension to a maximum stretch λ_{\max} of 3, showing only the pre-deformation and the third unload-reload loop. The elastic response σ_e (dashed line) and viscous response σ_v (dot-dash line) are obtained from the mean and from half of the difference between the third loop unloading and reloading stress, respectively. The transient portion of the data (here indicated as a strain of 0.33 at each end of the deformation) and the data used in the procedure are highlighted

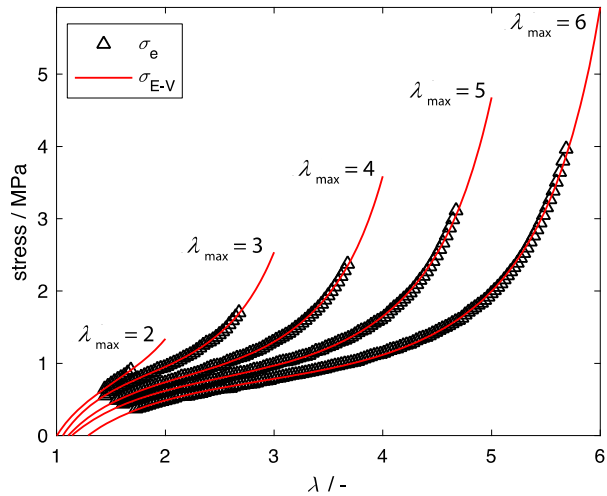


Following the ideas proposed by De Focatiis et al. (2009) and Prisacariu et al. (2005), σ_e and σ_v are computed from the experimental measurements as the mean and as half of the difference between the loading and the unloading stress, respectively. Here, to ensure that the viscoelastic transients have saturated, the initial and final 0.33 strains of each cycle are discarded. The elastic and viscous contributions obtained in this way are highlighted in Fig. 2.

3.2 Equilibrium contributions

The evolution of σ_e as a function λ , with increasing λ_{\max} , is illustrated in Fig. 3. The elastic response is strongly affected by the increase in historical maximum strain, and this implies that at least some of the Mullins effect arises from an evolution of the underlying elastic network, here simply dependent on λ_{\max} . Various hyperelastic models can be used to capture the elastomer's equilibrium response arising from the entropic nature of the network. In

Fig. 3 The experimental σ_e (symbols) and model σ_{E-V} (lines) equilibrium contributions as a function of stretch for five pre-deformation λ_{\max} levels between 2 and 6. The model is an Edwards-Vilgis function accounting for the permanent set λ_{set}



this instance, an Edwards-Vilgis (E-V) hyperelastic function (Edwards and Vilgis 1986) is chosen due to the physically inspired model parameters. The E-V strain energy density W function is given by

$$W = \frac{1}{2} N_C k_B T \left\{ \sum_i^3 \frac{\lambda_i^2 (1 - \alpha^2)}{1 - \alpha^2 \sum_i \lambda_i^2} + \log(1 - \alpha^2 \sum_i \lambda_i^2) \right\} + \frac{1}{2} N_S k_B T \sum_i^3 \left[\frac{\lambda_i (1 + \eta) (1 + \alpha^2)}{(1 + \eta \lambda_i^2) (1 - \alpha^2 \sum_i \lambda_i^2)} + \log(1 + \eta \lambda_i^2) \right] + \log(1 - \alpha^2 \sum_i \lambda_i^2) \quad (1)$$

where k_B is the Boltzmann constant, T is the absolute temperature, N_C is the cross-link density, N_S is the slip-link density, η is a measure of slip-link mobility, α is a measure of finite chain inextensibility and λ_i are the stretches in the principal directions.

The stress in the E-V spring can be determined by differentiation of Eq. (1) with respect to the stretch direction, accounting for isochoric deformation. E-V parameters were obtained by optimization on each third loop elastic contribution, and the process was repeated for all values of λ_{\max} . The optimization algorithm was coded in Matlab using the ‘lsqcurvefit’ tool to obtain values of N_C , N_S , α and η by minimization of the error, defined here as the root-mean-square (rms) of the difference between experimental and numerical stress values within one unload-reload loop. It was found that an E-V function on its own was unable to produce satisfactory fits to the data, and in order to achieve good agreement, it was necessary to incorporate a measure of permanent set λ_{set} , achieved via a multiplicative decomposition of λ into

$$\lambda = \lambda_{\text{set}} \lambda_{\text{eff}} \quad (2)$$

where λ_{eff} is the effective stretch, i.e. the stretch actually experienced by the network, and λ_{set} is a permanent plastic stretch arising from irreversible effects. In addition, N_C was always several orders of magnitude smaller than N_S , and hence insignificant as far as the total elastic stress is concerned. This is most likely due to the difficulty in separating the effects

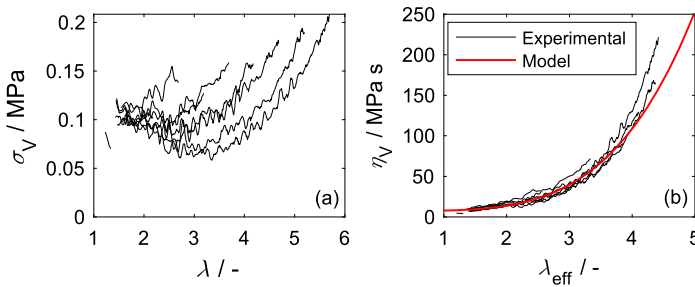


Fig. 4 (a) Viscous stress σ_V as a function of stretch λ , and (b) the viscosity η_V as a function of effective stretch λ_{eff} . When expressed as a function of λ_{eff} , the viscosity data overlay to form a master curve. A simple function is fitted to describe the viscosity master curve

of cross-links and slip-links. Hence, for the purpose of modeling the elastic response, it was sufficient to express the E-V function as

$$W = \frac{1}{2} N_s k_B T \sum_i^3 \left\{ \left[\frac{\lambda_{\text{eff},i} (1 + \eta) (1 + \alpha^2)}{(1 + \eta \lambda_{\text{eff},i}^2) (1 - \alpha^2 \sum \lambda_{\text{eff},i}^2)} + \log(1 + \eta \lambda_{\text{eff},i}^2) \right] + \log(1 - \alpha^2 \sum \lambda_{\text{eff},i}^2) \right\} \quad (3)$$

This combination produced excellent agreement between the elastic data and the E-V functions, as shown in Fig. 3, with rms errors typically of the order of 0.01 MPa, and always less than 0.02 MPa.

3.3 Viscous contributions

The viscous contribution to the stress σ_V is illustrated in Fig. 4a for all values of λ_{max} as a function of λ . The varying levels of λ_{max} lead to different σ_V vs. λ curves. This viscous contribution is associated with flow of the network, and, as such, a viscosity η_V is defined as

$$\eta_V = \frac{\sigma_{V,\text{true}}}{\dot{\epsilon}_{\text{true}}} \quad (4)$$

where $\sigma_{V,\text{true}}$ is the true flow stress and $\dot{\epsilon}_{\text{true}}$ is the true strain rate. It was found that σ_V differed with varying levels of λ_{max} , however, once λ_{set} obtained from the elastic optimization is accounted for, and η_V is plotted as a function of λ_{eff} , the curves overlap to form a single master curve as shown in Fig. 4b. The implication of this is that η_V may be modeled as a Mullins-independent, but λ_{eff} -dependent quantity. A plausible explanation for this effect is that molecular alignment leads to an increasingly anisotropic flow process. Similar effects have been noted in polymer glasses (De Focatiis and Buckley 2006; Senden et al. 2010).

Starting from the definition of true strain,

$$\epsilon_{\text{true}} = \ln(\lambda) = \ln(\lambda_{\text{eff}}) + \ln(\lambda_{\text{true}}) \quad (5)$$

the time derivative of Eq. (5) is calculated to determine $\dot{\epsilon}_{\text{true}}$ and is expressed as

$$\dot{\epsilon}_{\text{true}} = \frac{\dot{\lambda}}{\lambda} = \frac{\dot{\lambda}_{\text{eff}}}{\lambda_{\text{eff}}} + \frac{\dot{\lambda}_{\text{set}}}{\lambda_{\text{set}}} \quad (6)$$

where $\dot{\lambda}_{\text{eff}}$ is the effective stretch rate and $\dot{\lambda}_{\text{set}}$ is the rate of change of permanent set. The data used to determine the viscosity is obtained from the third loop. The evolution of λ_{set} predominantly takes place during the first loading, and it is assumed that $\dot{\lambda}_{\text{set}} = 0$ for subsequent loadings. Equation (6) is thus reduced to

$$\dot{\epsilon}_{\text{true}} = \frac{\dot{\lambda}}{\lambda} = \frac{\dot{\lambda}_{\text{eff}}}{\lambda_{\text{eff}}} \quad (7)$$

The relation between true $\sigma_{V,\text{true}}$ and nominal σ_V flow stresses can be expressed as $\sigma_{V,\text{true}} = \lambda \sigma_V$, and hence, by substitution of Eq. (7) into (4), η_V can be expressed as

$$\eta_V = \frac{\sigma_V \lambda \dot{\lambda}_{\text{eff}}}{\dot{\lambda}_{\text{eff}}} \quad (8)$$

4 Constitutive modeling

This section describes the implementation of a constitutive model incorporating the experimental observations stated above: (1) an additive decomposition of stress into elastic and viscous components; (2) the need for an effective stretch to account for permanent set; (3) network elasticity evolving with maximum stretch, and (4) a stretch-dependent viscosity. In addition, the behavior within viscoelastic transients will be considered to complete the model.

The proposed model, illustrated in Fig. 5, is a modified viscoelastic standard linear solid (SLS) model in series with a custom ‘slider’ element representing the permanent set. The modified SLS model consists of an E-V hyperelastic spring in parallel with a non-linear Maxwell element. The non-linearity of the Maxwell element arises from the non-linearity of the dashpot viscosity.

4.1 Model elements

4.1.1 Slider

In the proposed model, λ is decomposed into λ_{eff} and λ_{set} via a multiplicative decomposition as described in (2). The significance of λ_{eff} in this model is that it refers to the stretch that the E-V spring and the Maxwell element actually experience. The permanent set here represents the combined effects of irreversible deformation experienced by rubber and filler combined. It is modeled by a slider as shown on Fig. 5 whose stretch is, for the case of simple uniaxial deformation dealt with here, dependent on a monotonic function of λ_{max} . To cover more general cases this may need to be a more complex tensorial function of time, temperature and deformation history.

4.1.2 Non-linear Maxwell element

The viscoelastic behavior exhibited by the elastomer arises from local bond stiffness and viscous flow of monomer segments past each other and past the filler. Here it is modeled by a non-linear Maxwell element consisting of a linear elastic spring in series with a non-linear dashpot, as shown in Fig. 5. The governing differential equation for this element is

$$\dot{\sigma}_M + \frac{\sigma_M}{\tau} = \dot{\lambda}_{\text{eff}} E \quad (9)$$

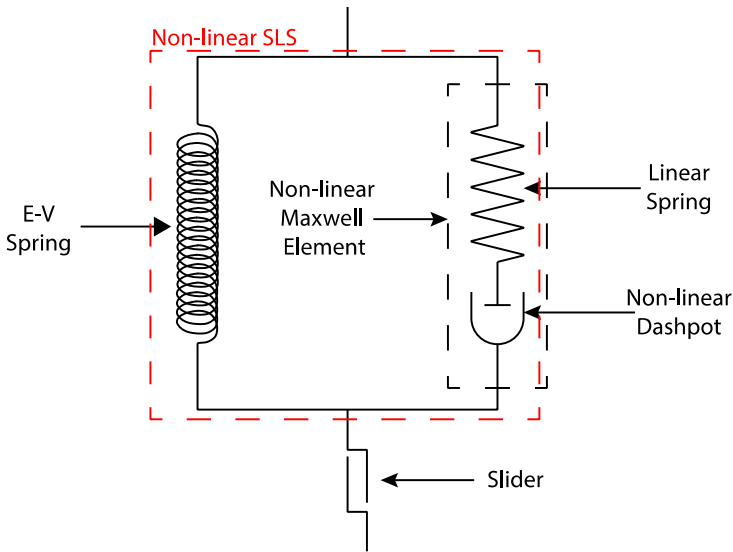


Fig. 5 A modified viscoelastic standard linear solid (SLS) model in series with a slider intended to represent permanent set. The SLS part of the model consists of an Edwards-Vilgis hyperelastic spring in parallel with a linear spring and a non-linear dashpot

where σ_M is the stress in the Maxwell element, $\dot{\sigma}_M$ is the stress rate, τ is a relaxation time, $\dot{\lambda}_{\text{eff}}$ is the effective stretch rate, and E is the stiffness of the linear spring. The relaxation time τ is given by $\eta_V / \lambda \dot{\lambda}_{\text{eff}} E$, where $\eta_V(\lambda_{\text{eff}})$ is the viscosity of the dashpot, which itself is a function of the effective stretch λ_{eff} , i.e. the viscosity master curve.

4.2 Parameter evolution

The values and uncertainties (expressed as 95% confidence intervals) of N_S , η , α and λ_{set} obtained from the optimizations carried out on the equilibrium contributions are illustrated on Fig. 6, for the full range of experiments carried out to different λ_{max} . At small values of λ_{max} , there is considerable uncertainty on these parameters due to the limited strain range of equilibrium data away from transients. All parameters exhibit a dependence on λ_{max} , suggesting that the maximum level of deformation influences all aspects of the elastic network. To describe this evolution, simple mathematical functions were fitted to the parameters as shown in Fig. 6, for values of $\lambda_{\text{max}} \geq 2.5$ only. Several forms of these functions were explored, and the functions selected are by no means unique, but provide simple and numerically stable representations of the parameter evolutions.

The forms of the functions selected to describe the evolution of the E-V parameters and of λ_{set} are

$$\log_{10}(N_S) = C_{1,N_S} \lambda_{\text{max}} + C_{2,N_S} \quad (10)$$

$$\alpha = C_{1,\alpha} \lambda_{\text{max}}^2 + C_{2,\alpha} \lambda_{\text{max}} + C_{3,\alpha} \quad (11)$$

$$\eta = C_{1,\eta} \exp(-C_{2,\eta} (\lambda_{\text{max}} - 1)) \quad (12)$$

$$\lambda_{\text{set}} = 1 + C_{1,\text{set}} (\exp(C_{2,\text{set}} \lambda_{\text{max}}) - \exp(C_{2,\text{set}})) \quad (13)$$

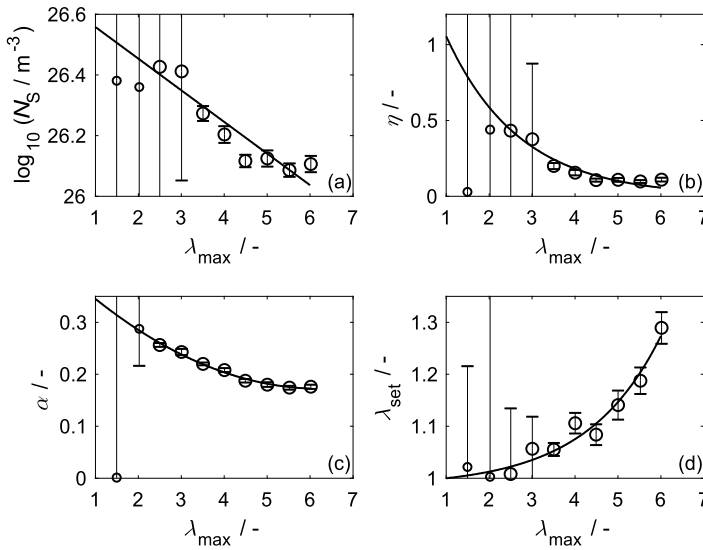


Fig. 6 The evolution of (a) slip-link density N_S , (b) slip-link mobility η , (c) chain inextensibility α and (d) permanent set λ_{set} with pre-deformation λ_{max} . The parameters extracted from the elastic contributions are shown as circles. The corresponding uncertainties (95% confidence interval) are also shown. To describe the evolution of these parameters, simple functions (lines) are fitted to the extracted parameter values as functions of λ_{max} for $\lambda_{max} \geq 2.5$ (larger circles)

Table 1 Estimate ± 1 standard uncertainty for the coefficients of Eqs. (10)–(14) describing the evolutions of the elastic parameters: slip-link density N_S , chain inextensibility α , slip-link mobility η , and of the permanent set λ_{set} , and of the viscosity η_V , as a function of maximum stretch λ_{max}

Parameters	Coefficients	
$\log_{10} N_S$	C_{1,N_S}	-0.104 ± 0.048
	C_{2,N_S}	26.662 ± 0.211
α	$C_{1,\alpha}$	0.006 ± 0.004
	$C_{2,\alpha}$	-0.079 ± 0.031
	$C_{3,\alpha}$	0.417 ± 0.063
η	$C_{1,\eta}$	1.055 ± 0.234
	$C_{2,\eta}$	0.586 ± 0.100
λ_{set}	$C_{1,set}$	0.009 ± 0.006
	$C_{2,set}$	0.577 ± 0.113
η_V	C_{1,η_V}	$(0.411 \pm 0.079) \text{ MPa s}$
	C_{2,η_V}	3.974 ± 0.148
	C_{3,η_V}	$(7.379 \pm 0.569) \text{ MPa s}$

To ensure that the permanent deformation is zero for virgin specimens, the condition $\lambda_{set} = 1$ at $\lambda_{max} = 1$ is applied to an exponential equation of the form $\lambda_{set} = C_{3,set} + C_{1,set} \exp(C_{2,set} \lambda_{max})$, resulting in expression (13). The estimates for the coefficients $C_{j,k}$ fitted to the data using linear regression for the functions are reproduced in Table 1.

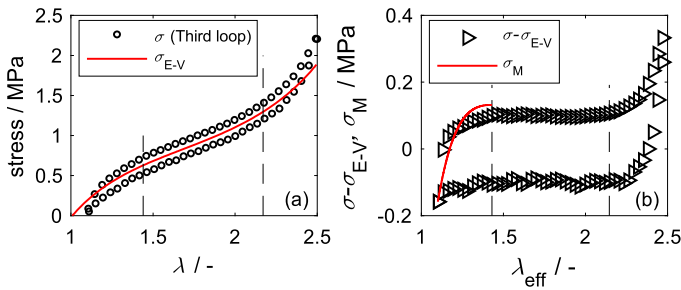


Fig. 7 (a) The experimental third loop response (symbols) for a pre-deformation λ_{\max} of 2.5 and the model elastic contribution σ_{E-V} (line). (b) Viscous contribution obtained by subtraction of the elastic stress obtained from the E-V model (symbols) from the total experimental stress, as a function of the effective stretch. The Maxwell model response σ_M (line) is obtained by solving numerically the governing equation for the non-linear Maxwell element (9) and optimizing for the spring stiffness. The vertical dashed lines are used to identify the transition between transient and steady-state portions of the data

4.3 Viscosity master curve

To describe the viscosity master curve as illustrated in Fig. 4b, a function of the form

$$\eta_V = C_{1,\eta_V} \lambda_{eff}^{C_{2,\eta_V}} + C_{3,\eta_V} \quad (14)$$

is proposed, and parameters are obtained by minimizing the normalized error and provided in Table 1.

Different approaches have been proposed to describe viscosity within a rubber constitutive model. These approaches often modify the dashpot element within a generalized Maxwell framework to capture inelastic effects, for example see the work of Rendek and Lion (2010), and Jalocha et al. (2015). Currently, to the best of the authors' knowledge, despite the experimental evidence suggesting a Mullins-independent but stretch-dependent viscosity, such an implementation has not been previously attempted for elastomers.

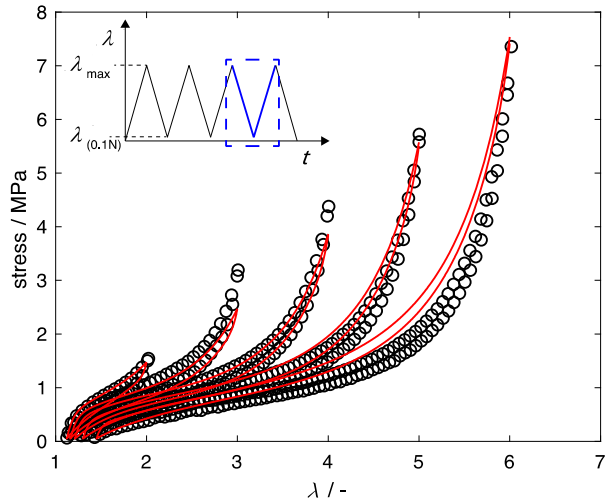
4.4 Determination of the linear spring modulus

The non-linear Maxwell element includes a linear elastic spring that, together with the non-linear dashpot, describes the transient response of the viscoelastic arm of the model. In order to determine E , the response within the transient regions must be considered. One can determine E via the numerical evaluation of Eq. (9) for the case of constant effective rate of deformation, where E is the only unknown.

The viscous contribution is obtained by subtracting the extrapolated elastic contribution predicted by the E-V model from the experimental third loop response within the transient, i.e. $\sigma - \sigma_{E-V}$. This is necessary because it is not possible to use the mean equilibrium experimental data within a transient. Fig. 7a illustrates an example of the third loop experimental data and the model elastic response extrapolated into the transients. The stress resulting from the subtraction process is shown in Fig. 7b.

In order to obtain a suitable value of E , the loading portion of σ_M is used in a least squares algorithm against a numerical solution for Eq. (9). This procedure was implemented on all experimental data sets to obtain $E = 3.07 \pm 1.09$ MPa. Fig. 7b shows an example of the experimental and model transient responses for the case $\lambda_{\max} = 2.5$. Although the agreement

Fig. 8 Comparison of experimental (symbols) and model (lines) third loop response for five pre-deformation λ_{\max} levels between 2 and 6. The inset shows the deformation history imposed on the specimens and the third unload-reload loop



between model and experiment is far from perfect, it should be noted that experimental data within the transients is noisy, and that for an accurate reproduction of the transients it is likely that a spectrum of relaxation times would be required.

A summary of the steps required in order to extract model parameters and their evolution is provided in Appendix A.

5 Results

5.1 Simulation of the third loop response

Once all model parameters have been obtained, they can be employed in generic simulations of the response. A comparison between the experimental and model third loop responses is shown on Fig. 8 for five λ_{\max} levels ranging from 2–6. Using a single set of model parameters, some of which evolve with λ_{\max} , simulation and experimental data are generally in good agreement, with the shape of the curves and the degree of permanent set matching reasonably well for all levels of stretch.

5.2 Simulation of more complex deformation histories

To probe the capability of the model, it was subjected to complex loading conditions probing cycles within a previously defined maximum stretch. Two protocols are employed, both of which condition the material by subjecting it to three cycles through to $\lambda = 4$. The first protocol (TP1) is followed by load/unload loops, where the specimen is loaded to increasing stretch levels and always unloaded (to 0.1N). The second protocol (TP2) starts at the maximum λ of 4, and unloads to progressively smaller λ , always reloading to $\lambda = 4$. The two protocols are shown in the insets of Figs. 9 and 10.

Comparisons between the experimental and the model responses for TP1 and TP2 are shown on Figs. 9 and 10, respectively. The primary loading is also shown here, and it can be seen that the model underestimates the stress in the latter stages of the loading. Beyond the

Fig. 9 A comparison between the experimental and model responses for TP1. The protocol consists of three uniaxial load/unload cycles, followed by five reload/unload loops and a reload/unload cycle, as shown in the inset. The dashed line in the inset represents the data that has been omitted from the plot

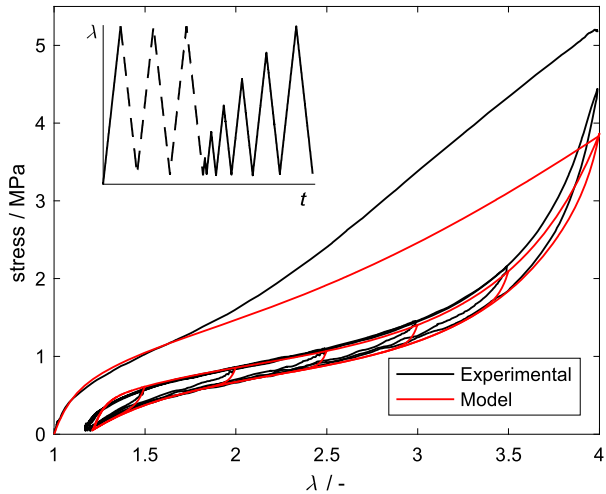
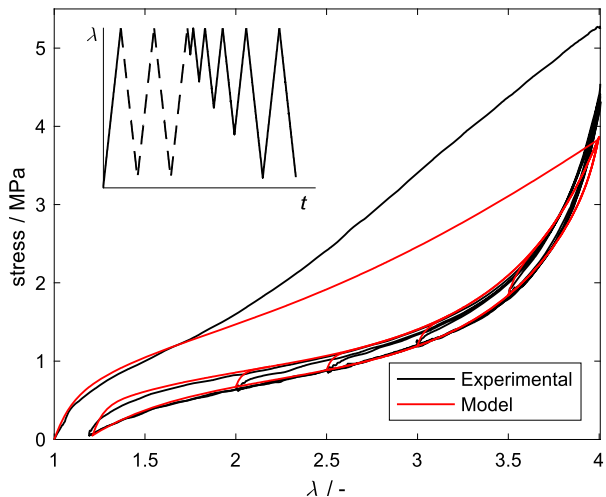


Fig. 10 A comparison between the experimental and model responses for TP2. The protocol consists of two uniaxial load/unload cycles, a reload step, four unload/reload loops, and lastly an unload/reload cycles and an unload step, as shown in the inset. The dashed line in the inset represents the data that has been omitted from the plot



initial loading, during the cycles, the model reproduces the stress well during the remaining deformation histories, although the transient responses saturate somewhat faster in the simulations compared to the experiments.

6 Discussion

6.1 Post-Mullins response

The model parameters were obtained by the use of cyclic experimental data sets, each of which remains within a pre-defined value of λ_{\max} . Thus, it is perhaps not surprising that the third unload-reload loops are reproduced to a good degree of accuracy. It should be noted, however, that the model does overestimate the stress for large values of λ_{\max} . This overestimation is attributed primarily to the combined inaccuracies arising from the functions

Fig. 11 A comparison of the experimental E_C^{exp} and model E_C^{mod} energy dissipated by the third loop

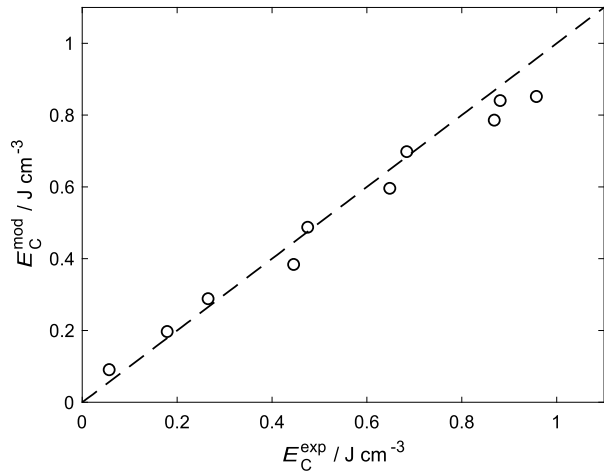
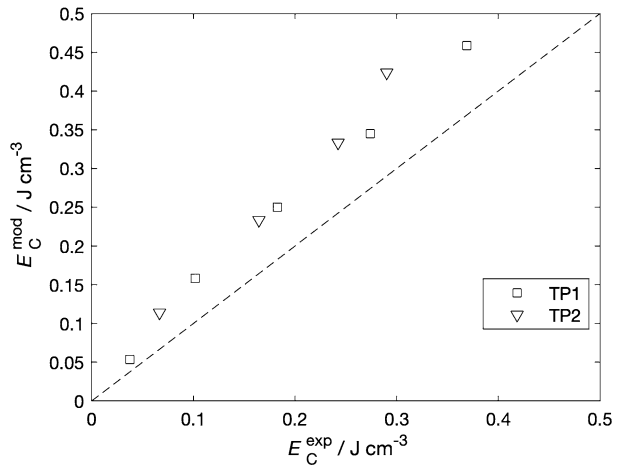


Fig. 12 Comparison between the dissipated energy obtained from experimental E_C^{mod} and model λ_{set} loops in complex loading histories TP1 and TP2



describing the evolution of the E-V parameters. It is possible that selection of more complex functions may lead to a better overall fit, but at the expense of an increase in the number of constants. What is particularly encouraging is the agreement in the energy dissipated per cycle between simulation E_C^{mod} and experiment E_C^{exp} , illustrated in Fig. 11. This is of interest in damping applications, and it shows that the model can accurately account for changes to dissipation arising as a result of changes to the constitutive behavior associated with the Mullins effect.

A further analysis of the dissipated energy can be obtained by considering the more complex deformation histories explored in Fig. 9 and Fig. 10. E_C^{mod} and E_C^{exp} are compared in Fig. 12, and again show generally a good level of agreement. The model overpredicts the energy dissipated by a small fraction, and this is attributed to the discrepancy in the transient behavior noted in Figs. 9 and 10.

6.2 Pre-Mullins response

Although the virgin loading response is never employed in obtaining the model parameters, it can be obtained from the model by extrapolation of the E-V parameters to zero strain. This allows for a comparison between the model and experimental first loading as highlighted on Figs. 9 and 10. It is apparent that there is an increasing discrepancy in the stress for $\lambda > 2$, and the model underpredicts the stress during the first loading. It is plausible that the changes occurring when the material is exceeding its previous λ_{\max} (i.e. when $\dot{\lambda}_{\text{set}} > 0$ and model parameters are evolving) might themselves be associated with a dissipative and time-dependent process. This would not be surprising since there is evidence in the literature of Mullins healing (Corby and De Focatiis 2019).

In line with the above idea, one approach to achieving a larger stress during the first loading could be to include an additional viscosity dependent on $\dot{\lambda}_{\text{set}}$. A stress defined in this way would only be present during the initial loading stage, and hence not impact the rest of the simulations.

6.3 Extension to a fully three-dimensional model

In principle, the only major obstacles to a fully three-dimensional (3D) implementation of the proposed model concern the description of permanent set, of the elastic parameter evolution, and of a suitable effective stretch scalar, all of which are possible. It is well known, however, that both processing and deformation of elastomers can lead to anisotropic behavior (Diani et al. 2009; Fernandes and De Focatiis 2015; Mullins 1949). Constitutive models ought to accommodate this induced anisotropy, which will undoubtedly affect not only the elastic part but also the viscosity and the permanent set. This would require a much more extensive experimental data set involving sequential straining in different directions to identify where simplifications might be made in order to reduce the number of material constants. Typically, the notion of material directions is used to tackle anisotropy, for example see work by Göktepe and Miehe (2005), Diani et al. (2006), Itskov et al. (2010), Merkel et al. (2013) and Rebouah et al. (2013).

It is worth noting that, in an early study by Mullins (1949), when sheets of elastomers were subjected to sequential deformations in two perpendicular directions it was found that: (1) the ratio between the permanent sets in the alternating directions remained constant, largest in the direction of stretch; and, (2) the permanent deformation remained isochoric. It is therefore plausible that a significant part of the observed anisotropy could be attributed to permanent deformation alone, and that an isotropic (but evolving) hyperelastic formulation coupled with a simple 3D representation of permanent set might suffice in a generic 3D implementation. Work is on-going in our laboratory to assemble a 3D model based on this hypothesis.

7 Conclusions

This study has described how a constitutive model can be assembled on the basis of observations made from the separation of elastic and viscous contributions in uniaxial cyclic tensile experiments on EPDM rubber. The model includes a description of the evolution of both permanent set and hyperelastic parameters of an Edwards-Vilgis function to account for the Mullins effect. The novelty of this model arises from the use of a viscosity master curve to describe the non-linear Mullins-independent but strain-dependent flow stress, which was

obtained directly from the viscous contribution from the experimental data. The approach described also presents a straightforward route to obtaining the relevant parameters from cyclic experimental data.

The model reproduces the cyclic response of the deformation histories explored in this study to a good level of accuracy. The model is also able to accurately predict the dissipated energy per cycle and its change with increasing levels of pre-deformation. Where cycles are smaller in amplitude, and the dissipated energy is more influenced by transients, the accuracy of the predictions is reduced since the model employs a single relaxation time.

When the prediction of the initial loading is compared to experimental data, the model underestimates the stress at larger strain levels. In practical applications, where elastomeric products are often scragged (i.e., subjected to pre-deformation), this limitation is less relevant, and the focus is always on the cyclic response, and how it changes with different scragging levels, something which the model predicts well.

Acknowledgement The authors wish to acknowledge the contribution of Dr. T. Alshuth of the German Institute of Rubber Technology (DIK) in supplying the EPDM rubber material.

Publisher's Note Springer Nature remains neutral with regard to jurisdictional claims in published maps and institutional affiliations.

Open Access This article is licensed under a Creative Commons Attribution 4.0 International License, which permits use, sharing, adaptation, distribution and reproduction in any medium or format, as long as you give appropriate credit to the original author(s) and the source, provide a link to the Creative Commons licence, and indicate if changes were made. The images or other third party material in this article are included in the article's Creative Commons licence, unless indicated otherwise in a credit line to the material. If material is not included in the article's Creative Commons licence and your intended use is not permitted by statutory regulation or exceeds the permitted use, you will need to obtain permission directly from the copyright holder. To view a copy of this licence, visit <http://creativecommons.org/licenses/by/4.0/>.

Appendix A: Summary of parameter identification strategy

Handling experimental data:

1. Decompose the third loop of the uniaxial cyclic data into σ_e and σ_v .
2. Discard the transient portions of σ_e and σ_v .

Identification of E-V parameters and λ_{set} :

3. Fit the derivative of W (Eq. (3)) with respect to λ_{eff} to σ_e for all values of λ_{max} explored.
4. Select and fit appropriate functions (Eq. (10)–(13)) to describe the evolution of E-V parameters and λ_{set} .

Identification of the viscosity master curve

5. $\eta_v (= \sigma_{v,true} / \dot{\lambda}_{true})$ forms a master curve when λ_{set} is accounted for.
6. Fit an appropriate function (Eq. (14)) to describe the evolution of viscosity.

Identification of E :

7. Consider the transient portions discarded in step 2.
8. Subtract from the transient portion the elastic response predicted by the E-V model.
9. Minimise the rms error between the experimental data and the numerical solution to Eq. (9) at a constant effective rate of deformation to identify E .

References

- Bergström, J.S.S., Boyce, M.C.C.: Constitutive modeling of the large strain time-dependent behavior of elastomers. *J. Mech. Phys. Solids* **46**, 931–954 (1998). [https://doi.org/10.1016/S0022-5096\(97\)00075-6](https://doi.org/10.1016/S0022-5096(97)00075-6)
- Clough, J.M., Creton, C., Craig, S.L., Sijbesma, R.P.: Covalent bond scission in the Mullins effect of a filled elastomer: real-time visualization with mechanoluminescence. *Adv. Funct. Mater.* **26**, 9063–9074 (2016). <https://doi.org/10.1002/adfm.201602490>
- Corby, M., De Focatiis, D.S.A.: Reversibility of the Mullins effect for extending the life of rubber components. *Plast. Rubber Compos.* **48**, 24–31 (2019). <https://doi.org/10.1080/14658011.2018.1443384>
- De Focatiis, D.S.A., Buckley, C.P.: The initiation of environmental stress crazes in polystyrene with process induced anisotropy. In: Proceedings of the 22nd Annual Meeting of the Polymer Processing Society, 2–6 July 2006, Yamagata, Japan (2006)
- De Focatiis, D.S.A., Buckley, C.P., Abraham, F.: Multiaxial viscoelastic deformation of carbon-black filled EPDM rubber. In: Heinrich, G., Kaliske, M., Lion, A., Reese, S. (eds.) *Constitutive Models for Rubber VI*, pp. 187–192. Taylor & Francis, Dresden (2009)
- Diani, J., Brieu, M., Gilormini, P.: Observation and modeling of the anisotropic visco-hyperelastic behavior of a rubberlike material. *Int. J. Solids Struct.* (2006). <https://doi.org/10.1016/j.ijsolstr.2005.06.045>
- Diani, J., Fayolle, B., Gilormini, P.: A review on the Mullins effect. *Eur. Polym. J.* **45**, 601–612 (2009). <https://doi.org/10.1016/j.eurpolymj.2008.11.017>
- Dorfmann, A., Ogden, R.W.: A constitutive model for the Mullins effect with permanent set in particle-reinforced rubber. *Int. J. Solids Struct.* **41**, 1855–1878 (2004). <https://doi.org/10.1016/j.ijsolstr.2003.11.014>
- Edwards, S.F., Vilgis, T.: The effect of entanglements in rubber elasticity. *Polym. Commun. (Guildf.)* **27**, 483–492 (1986). [https://doi.org/10.1016/0032-3861\(86\)90231-4](https://doi.org/10.1016/0032-3861(86)90231-4)
- Fernandes, V.A.: Manifestations of the Mullins effect in filled elastomers (2016). <http://eprints.nottingham.ac.uk/32301/>
- Fernandes, V.A., De Focatiis, D.S.A.: A swelling study of process-induced and deformation-induced anisotropy of filled rubbers. In: *Const. Model. Rubbers IX*, pp. 141–146 (2015). <https://doi.org/10.1201/b18701-28>
- Fukahori, Y.: New progress in the theory and model of carbon black reinforcement of elastomers. *J. Appl. Polym. Sci.* **95**, 60–67 (2005). <https://doi.org/10.1002/app.20802>
- Göktepe, S., Miehe, C.: A micro-macro approach to rubber-like materials. Part III: the micro-sphere model of anisotropic Mullins-type damage. *J. Mech. Phys. Solids* **53**, 2259–2283 (2005). <https://doi.org/10.1016/j.jmps.2005.04.010>
- Hanson, D.E., Hawley, M., Houlton, R., Chitanvis, K., Rae, P., Orlor, E.B., Wroblewski, D.A.: Stress softening experiments in silica-filled polydimethylsiloxane provide insight into a mechanism for the Mullins effect. *Polym. Commun. (Guildf.)* **46**, 10989–10995 (2005). <https://doi.org/10.1016/j.polymer.2005.09.039>
- Haward, R.N., Thackray, G.: The use of a mathematical model to describe isothermal stress-strain curves in glassy thermoplastics. *Proc. R. Soc. A, Math. Phys. Eng. Sci.* **302**, 453–472 (1968). <https://doi.org/10.1098/rspa.1968.0029>
- Houwink, R.: Slipping of molecules during the deformation of reinforced rubber. *Rubber Chem. Technol.* **29**, 888–893 (1956). <https://doi.org/10.5254/1.3542602>
- Itskov, M., Ehret, A.E., Kazakevičiute-Makovska, R., Weinhold, G.W.: A thermodynamically consistent phenomenological model of the anisotropic Mullins effect. *Z. Angew. Math. Mech.* (2010). <https://doi.org/10.1002/zamm.200900279>
- Jalocha, D., Constantinescu, A., Neviere, R.: Prestrain-dependent viscosity of a highly filled elastomer: experiments and modeling. *Mech. Time-Depend. Mater.* **19**, 243–262 (2015). <https://doi.org/10.1007/s11043-015-9262-z>
- Kraus, G., Childers, C.W., Rollmann, K.W.: Stress softening in carbon black-reinforced vulcanizates. Strain rate and temperature effects. *J. Appl. Polym. Sci.* **10**, 229–244 (1966). <https://doi.org/10.1002/app.1966.070100205>
- Maher, E., Creane, A., Lally, C., Kelly, D.J.: An anisotropic inelastic constitutive model to describe stress softening and permanent deformation in arterial tissue. *J. Mech. Behav. Biomed. Mater.* **12**, 9–19 (2012). <https://doi.org/10.1016/j.jmbbm.2012.03.001>
- Marckmann, G., Verron, E., Gornet, L., Chagnon, G., Charrier, P., Fort, P.: A theory of network alteration for the Mullins effect. *J. Mech. Phys. Solids* **50**, 2011–2028 (2002). [https://doi.org/10.1016/S0022-5096\(01\)00136-3](https://doi.org/10.1016/S0022-5096(01)00136-3)
- Merckel, Y., Diani, J., Brieu, M., Caillard, J.: Constitutive modeling of the anisotropic behavior of Mullins softened filled rubbers. *Mech. Mater.* (2013). <https://doi.org/10.1016/j.mechmat.2012.10.010>

- Mullins, L.: Effect of Stretching on the Properties of Rubber (1948). <http://rubberchemtechnol.org/doi/abs/10.5254/1.3546914?journalCode=rcat>
- Mullins, L.: Permanent set in vulcanized rubber. *Rubber Chem. Technol.* **22**, 1036–1044 (1949). <https://doi.org/10.5254/1.3543010>
- Mullins, L., Tobin, N.R.: Theoretical model for the elastic behavior of filler-reinforced vulcanized rubbers. *Rubber Chem. Technol.* **30**, 555–571 (1957). <https://doi.org/10.5254/1.3542705>
- Mullins, L., Tobin, N.R.: Stress softening in rubber vulcanizates. Part I. Use of a strain amplification factor to describe the elastic behavior of filler-reinforced vulcanized rubber. *J. Appl. Polym. Sci.* **9**, 2993–3009 (1965). <https://doi.org/10.1002/app.1965.070090906>
- Peña, E.: Computational aspects of the numerical modelling of softening, damage and permanent set in soft biological tissues. *Comput. Struct.* **130**, 57–72 (2014). <https://doi.org/10.1016/j.compstruc.2013.10.002>
- Prisacariu, C., Buckley, C.P., Caraculacu, A.A.: Mechanical response of dibenzyl-based polyurethanes with diol chain extension. *Polym. Commun. (Guildf.)* **46**, 3884–3894 (2005). <https://doi.org/10.1016/j.polymer.2005.03.046>
- Qi, H.J., Boyce, M.C.: Constitutive model for stretch-induced softening of the stress-stretch behavior of elastomeric materials. *J. Mech. Phys. Solids* **52**, 2187–2205 (2004). <https://doi.org/10.1016/j.jmps.2004.04.008>
- Rebouah, M., Machado, G., Chagnon, G., Favier, D.: Anisotropic Mullins stress softening of a deformed silicone holey plate. *Mech. Res. Commun.* (2013). <https://doi.org/10.1016/j.mechrescom.2013.02.002>
- Rendek, M., Lion, A.: Amplitude dependence of filler-reinforced rubber: experiments, constitutive modelling and FEM—implementation. *Int. J. Solids Struct.* **47**, 2918–2936 (2010). <https://doi.org/10.1016/j.ijsolstr.2010.06.021>
- Senden, D.J.A., Van Dommelen, J.A.W., Govaert, L.E.: Strain hardening and its relation to Bauschinger effects in oriented polymers. *J. Polym. Sci., Part B, Polym. Phys.* (2010). <https://doi.org/10.1002/polb.22056>
- Simo, J.C.: On a fully three-dimensional finite-strain viscoelastic damage model: formulation and computational aspects. *Comput. Methods Appl. Mech. Eng.* **60**, 153–173 (1987). [https://doi.org/10.1016/0045-7825\(87\)90107-1](https://doi.org/10.1016/0045-7825(87)90107-1)